Chinese Journal of
POLYMER SCIENCE

RESEARCH ARTICLE

https://doi.org/10.1007/s10118-026-3757-8
Chinese J. Polym. Sci.

Multi-stimuli Responsive Polyurethane-based Materials: Structure-Property Correlations

Yi-Sheng Huang, Han-Xin Jian, Hao Huang, Qing-Yun Guo*, and Shu-Guang Yang*

State Key Laboratory of Advanced Fibers Materials, Center for Advanced Low-dimension Materials, College of Materials Science and Engineering, Donghua University, Shanghai 201620, China

Electronic Supplementary Information

Abstract Heat-, light-, and humidity-responsive materials were fabricated *via* chemical design and cold drawing processing. The crystallizable polyether/polyester diols were first reacted with isophorone diisocyanate (IPDI), followed by chain extension with azobenzene units. The synthesized polyurethanes exhibited ductile behavior and drawing-induced orientation when the soft segments possessed high crystallinity. Upon heating or UV irradiation, the oriented polyurethane strips underwent bending, whereas the pristine strips did not. Under humid conditions, both oriented and pristine polyurethane strips containing poly(ethylene oxide) (PEO) soft segments bent, albeit in opposite directions. In contrast, polyurethane strips with polycaprolactone (PCL) and polytetramethylene ether glycol (PTMEG) soft segments showed no response to humidity, regardless of whether they were stretched. Mechanistic investigations revealed that the temperature increase resulting from the photothermal effect of the azobenzene moieties is the main reason for light-induced actuation, which differs from that in many other azobenzene-based materials. The entropic elastic energy stored during stretching is released upon UV irradiation, heating, or humidification to drive the bending deformation. This work presents a strategy for constructing multi-stimuli- responsive materials *via* molecular design and post-processing, highlighting the synergy between functional moieties and microscopic structures, which holds great significance for the development of advanced intelligent materials.

Keywords Polymer crystallization; Polyurethanes; Humidity sensitivity; Photothermal effect; Stimuli-responsive materials

Citation: Huang, Y. S.; Jian, H. X.; Huang, H.; Guo, Q. Y.; Yang, S. G. Multi-stimuli responsive polyurethane-based materials: structure-property correlations. *Chinese J. Polym. Sci.* https://doi.org/10.1007/s10118-026-3757-8

INTRODUCTION

Stimuli-responsive polymers, or "smart" polymers, which can undergo alterations in solubility, volume, and/or conformation in response to external stimuli, have attracted considerable attention for advanced applications, such as optoelectronic devices,[1–4] energy storage,[5] smart textiles,[6,7] soft robotics,[8–12] and flexible electronics.[13–16] To realize the responsiveness of polymeric materials towards multi-stimuli, the fundamental principle is to introduce functional moieties responsive to different stimuli,[17–20] such as light,[21] temperature,[22] pH value,[23] humidity,[24] electrical field,[25] and chemical stimuli,[26] into polymer structures. When different stimuli are applied, diverse stimuli-sensitive moieties integrated within a single polymer can exhibit multifarious responsive behavior.[27] For instance, photochromic azobenzene moieties have been incorporated into the copolymer of *N*-isopropylacrylamide (NIPAM) with *N*-(4-phenylazophenyl)acrylamide,[28] yielding a material that exhibits dual responsiveness to both light and heat. Triple-stimuli and even quadruple-stimuli-responsive materials have been proposed and elaborately illustrated in aqueous systems.[29–35]

In nature, organisms such as plants, spider webs, and muscles exhibit hierarchically ordered architectures *via* biological self-organization, which endows them with multifunctional capabilities that enable responses to complex environments, including mechanical reinforcement, environmental protection, stimuli-responsive actuation, and efficient mass transport.[36–39] Inspired by spider silk, researchers have developed various advanced materials, including robust double cross-linked networks (DCNs) utilizing slide-ring molecules,[40] twisted thermo-responsive polyurea fibers with twistocaloric cooling,[41] and healable and recyclable supramolecular elastomers.[42] These bio-inspired systems demonstrate that converting external stimuli into programmable deformations is the key to designing responsive polymer materials. This can be achieved by incorporating stimuli-responsive polymers—macromolecules designed to undergo significant changes in their physical or chemical properties upon receiving a specific signal—into materials with specific structures.[43–49] Azobenzene undergoes *trans-cis* isomerization when irradiated with light of an appropriate wavelength. Reverse *cis-trans*

* Corresponding authors, E-mail: guoqy@dhu.edu.cn (Q.Y.G.)
E-mail: shgyang@dhu.edu.cn (S.G.Y.)
Received April 20, 2026; Accepted May 27, 2026; Published online July 22, 2026

isomerization can be driven by light or occurs thermally in the dark. The photochromatic properties of azobenzene make it an ideal component for numerous molecular devices and functional materials. The design and construction of numerous azobenzene-containing functional structures have been extensively studied.[50,51] Azobenzene derivatives were incorporated into a polyurethane system and it was found that poly(urethane-urea) (PUU) materials bearing azobenzene moieties and an oriented structure exhibited light-stimuli-responsive bending deformation, indicating that molecular orientation plays a decisive role in regulating and enhancing the stimuli-responsive performance.[52] Despite the well-established research framework of polyurethane as a versatile high-performance polymer and extensive research efforts dedicated to stimuli-responsive polyurethanes,[53] there remains an urgent need to establish a fundamental and systematic cognitive framework for how the precise chemical microenvironment governs the macroscopic responsive behavior.

In this study, we fabricated multi-stimuli-responsive polymeric materials using a combination of chemical synthesis to incorporate functional moieties and physical processing to induce orientation. Poly(ethylene glycol) (PEG), poly(tetramethylene ether) glycol (PTMEG), and poly(ε-caprolactone) diol (PCL) soft segments with distinct hydrophilicity and crystallization behaviors and photoresponsive azobenzene groups were incorporated into the polyurethane chains *via* chemical synthesis. Polyurethane chains have multi-block architectures with micro-phase separation.[54,55] When the soft segments are highly crystalline with melting points above room temperature, the polyurethanes become ductile. Oriented microstructures of ductile polyurethanes can be developed *via* cold drawing, thereby enhancing the photoresponsive and thermoresponsive behaviors but reducing the humidity sensitivity compared to unoriented samples. The prepared polyurethane materials exhibited heat-, light-, and humidity-responsive behaviors with stimuli-sensitive moieties and well-oriented microstructures.

EXPERIMENTAL

Materials

Poly(ε-caprolactone) diol (PCL, M_n=4000 g·mol^{-1}) was purchased from Wuhan Kemic Biomedical Technology Co., Ltd., polytetramethylene ether glycol (PTMEG, M_n=4000 g·mol^{-1}) from Jining Benock Biotechnology Co., Ltd., and polyethylene glycol (PEO, M_n=4000 g·mol^{-1}) from Shanghai Titan Scientific Co., Ltd. Isophorone diisocyanate (IPDI), 4,4′-dihydroxyazobenzene (DHAB), and 4,4′-azodianiline (ADA) were obtained from Shanghai Titan Scientific Co., Ltd.

Synthesis of Polyurethanes

In a nitrogen-filled atmosphere, PEG, PTMEG, or PCL diols (2.5 mmol) were placed in a dry three-necked flask, heated to 110 °C under vacuum, and stirred vigorously for 4 h to eliminate residual moisture. Once cooled to 75 °C, 10 mL of dimethylacetamide (DMAc) solution of 5.1 mmol of IPDI and 0.03 g of dibutyltin dilaurate (DBTDL) catalyst was added slowly, followed by being stirred at 75 °C for another 4 h. Subsequently, the system was cooled to 40 °C, and 2.6 mmol of azobenzene chain extender (ADA or DHAB)—dissolved in 10 mL of DMAc/*N*,*N*-dimethylformamide (DMF) (8/2, *V*/*V*)—was added. The reaction mixture was stirred at 40 °C for 24 h. Finally, the reaction mixture was heated to 75 °C and maintained for approximately 6 h, yielding a yellow viscous product. The polymer was purified *via* precipitation with cold ether to remove oligomers, unreacted materials, and catalyst, followed by drying under vacuum at 70 °C for 12 h.

Gel Permeation Chromatography

Gel permeation chromatography (GPC) analyses were performed using an LC-100 HP pump (Shanghai Wufeng Scientific Instrument Co., Ltd.), a Mono GPC-100 column (7.8 × 300 mm, 5 μm, 1000 Å; Sepax Technologies, Inc.), and a Shodex RI-201H refractive index detector (Shoko Science Co., Ltd.). The mobile phase consisted of *N*,*N*-dimethylformamide (DMF) delivered at a flow rate of 1.0 mL·min^{-1}, and the column temperature was maintained at 40 °C. Relative molecular weights and molecular weight distributions were determined using polystyrene standards. Data acquisition and processing were performed using a V2008GPC software package installed on a dedicated workstation.

UV-Visible (UV-Vis) Spectroscopy

UV-Vis absorption spectra were acquired on a PerkinElmer Lambda 950 spectrophotometer. Samples of polyurethanes were dissolved in DMF at a concentration of approximately 0.05 mg/mL and loaded into standard 1.0 cm path length quartz cuvettes. After irradiation for various durations using a UV lamp (UVGO, 365 nm, 45 W, AC 90–240 V), the spectra were immediately recorded in a dark compartment to prevent any unintended photochemical effects during measurement.

Differential Scanning Calorimetry

Differential scanning calorimetry (DSC) measurements were conducted on a Discovery DSC 250 instrument (TA Instruments, USA). Prior to analysis, the samples were dried in an oven at 40 °C for 24 h and subsequently hermetically sealed in Tzero aluminum pans. The thermal protocol involved heating the samples from 25 °C to 120 °C, followed by cooling to –70 °C and a second heating scan to 120 °C. All heating/cooling processes were performed at a constant rate of 10 °C·min^{-1} under a nitrogen purge of 50 mL·min^{-1}. The crystallization temperature (T_c) and melting temperature (T_m) were determined from the peak positions of the cooling and second-heating scans, respectively. The crystallinity χ_c of all samples was calculated based on the melting enthalpy, as shown in Eq. (1):

$$\chi_c = \frac{\Delta H_m}{\Delta H_m^{\infty}} \times \frac{1}{W_c} \times 100\% \quad (1)$$

where ΔH_m is the measured melting enthalpy of crystalline segment; ΔH_m^{∞} is the melting enthalpy of the 100% crystalline PEG, PTMEG, or PCL; and W_c is the weight fraction of PEG, PTMEG, or PCL in PU.

Tensile Testing

The tests were conducted at 25 °C and 50 RH% using a tensile machine (UTM2502, Suns, China). Each sample was measured at least five times, at a stretching rate of 10 mm·min^{-1}. Engineering stress (σ), engineering strain (ε), drawing ratio (λ) and deformation length keeping ratio (R_L) were described by the following equations:

https://doi.org/10.1007/s10118-026-3757-8

$$\sigma = \frac{F}{S} \quad (2)$$

$$\varepsilon = \frac{L - L_0}{L_0} \quad (3)$$

$$\lambda = \frac{L}{L_0} = 1 + \varepsilon \quad (4)$$

$$R_L = \frac{L_t - L_0}{\lambda L_0 - L_0} \quad (5)$$

where F is the tensile force, S is the cross-sectional area, L is the drawing length, L_0 is the pristine length, L_t is the length after removing the stress.

Thermal Imaging Characterization

Real-time thermal evolution of the film strips (14.54 mm × 8.29 mm × 0.214 mm) during actuation was monitored using a high-resolution IR camera (FLIR T1050sc, 1024×768 pixels, emissivity: 0.35) at 20 °C and 40% RH. Photothermal testing utilized unilateral 365 nm UV irradiation (200 mW·cm^{-2}) from a 5 cm distance.

RESULTS AND DISCUSSION

Azobenzene-containing polyurethanes were synthesized using a two-step procedure. First, polyether/polyester diols (PCL, PEO, or PTMEG) were reacted with excess IPDI to form isocyanate-terminated prepolymers. These prepolymers were subsequently chain-extended using azobenzene derivatives, namely 4,4′-azodianiline (ADA) or 4,4′-dihydroxyazobenzene (DHAB) (Scheme 1a). The compositions and molecular weights of the resulting polyurethanes are summarized in Scheme 1. The detailed synthetic routes, procedures, and characterization data are provided in the electronic supplementary information (ESI).

Differential scanning calorimetry (DSC) was performed to evaluate the thermal behavior of the synthesized PUs (Fig. 1). All polyurethanes and their corresponding unreacted diols were characterized to enable comparative analysis. Table 1 summarizes the melting temperature (T_m), crystallization temperature (T_c), and crystallinity (χ_c) of these polyether/polyester diols, which exhibit significant differences from their corresponding polyurethane derivatives. Upon the incorporation of diols into the polyurethane backbone, significant reductions in crystallinity, T_m, and T_c were observed. For instance, neat PEO-4k exhibited a T_m of 60 °C and a T_c of 36 °C (Fig. 1a); however, these values decreased to 46 °C and 23 °C, respectively, for EPA and EPH (Fig. 1b). Consistent with this trend, the χ_c of PEO in EPA and EPH are 33.0% and 42.7%, respectively—much lower than that of neat PEO-4k (77.8%). PEO-4k, as a short flexible chain in its neat state, avoids entanglement, allowing its chains to align freely into ordered spherulites or lamellae, resulting in high crystallinity. In contrast, EPA and EPH are formed *via* irreversible covalent bonding between PEO soft segments and hard segments through the isocyanate groups of IPDI *via* rigid linkers, which restrict the motion of soft segment chain ends, hindering the parallel alignment of PEO chains into the crystalline domains. Furthermore, these multi-block copolymers undergo thermodynamically driven microphase separation: rigid hard segments spontaneously aggregate into hard-segment microdomains *via* hydrogen bonds. These microdomains further compress the effective crystallization space of the PEO soft segments and restrict the rotation and extension of the PEO chains, precluding a sufficiently ordered arrangement into crystals. Both effects collectively explain the lower crystallinity and melting points of PEO in the polyurethanes compared to neat PEO-4k.

During the first cooling cycle, the crystallization peaks of TPA and CPA were observed at approximately 0 and −4 °C, respectively. In contrast, TPH and CPH exhibited crystallization peaks at approximately 10 °C, which were notably higher than those of their "A" counterparts. Meanwhile, Both EPA and EPH exhibited crystallization peaks near 20 °C. Upon subsequent heating, all six compounds—EPA, EPH, TPA, TPH, CPA, and CPH—displayed endothermic melting peaks at approximately 46 °C. The observed crystallization behavior of these polyurethanes was governed by the interplay between the intrinsic crystallizability of the soft segments and the microphase structure dictated by the hard segments. Among the soft segments employed, poly(ethylene oxide) (PEO) possesses a highly regular, symmetrical repeating unit with a short sequence length, which strongly favors parallel chain packing and rapid crystallization. Consequently, EPA and EPH—both with PEO soft segments, exhibit the highest crystallization temperatures (about 20 °C) in the series. Poly(ε-caprolactone) (PCL), while maintaining a linear backbone, incorporates ester groups that disrupt structural symmetry and reduce overall regularity; therefore, its intrinsic crystallizability is lower than that of PEO. Poly(tetramethylene ether glycol) (PTMEG) features an extended carbon chain between ether linkages, which further diminishes the molecular regularity and retards long-range ordered alignment. In addition to the soft segments, the hard segments exert a non-negligible effect on the thermal behavior. In CPH, the hard segments are constructed from aromatic diphenol chain extenders that promote strong π–π stacking and cohesive urethane–urethane hydrogen bonds. This leads to a high degree of microphase separation, yielding well-defined hard domains that efficiently exclude the PCL segments. The resulting PCL soft domains are relatively "pure," with few hard segment intrusions. Their chains retain high segmental mobility and can readily undergo conformational adjustment and orderly packing upon cooling. As a result, CPH exhibited a high crystallization peak temperature with a pronounced exotherm. In contrast, CPA contains hard segments that are rich in urea linkages. These urea groups form strong hydrogen bonds with the ester groups of PCL, whereas the rigid phenyl rings and urea units dispersed in the soft domains act as physical cross-links and steric hindrances. This severe phase mixing restricts the segmental motion of PCL chains so substantially that effective chain folding and ordered packing are kinetically hindered. Crystallization is thus forced to proceed only at much lower temperatures, where a large supercooling provides a sufficient thermodynamic driving force to overcome the constraints. Correspondingly, the crystallization peak temperature of CPA was markedly depressed (to approximately −5 °C). This difference in microphase separation strength can be further validated by SAXS (Fig. S8 c in ESI). For PEO-based polyurethanes, the extremely strong crystallization tendency of PEO dominates, so that even variations in the hard segment structure produce only minor shifts in the crystallization temperature; however, the same trend holds,

a

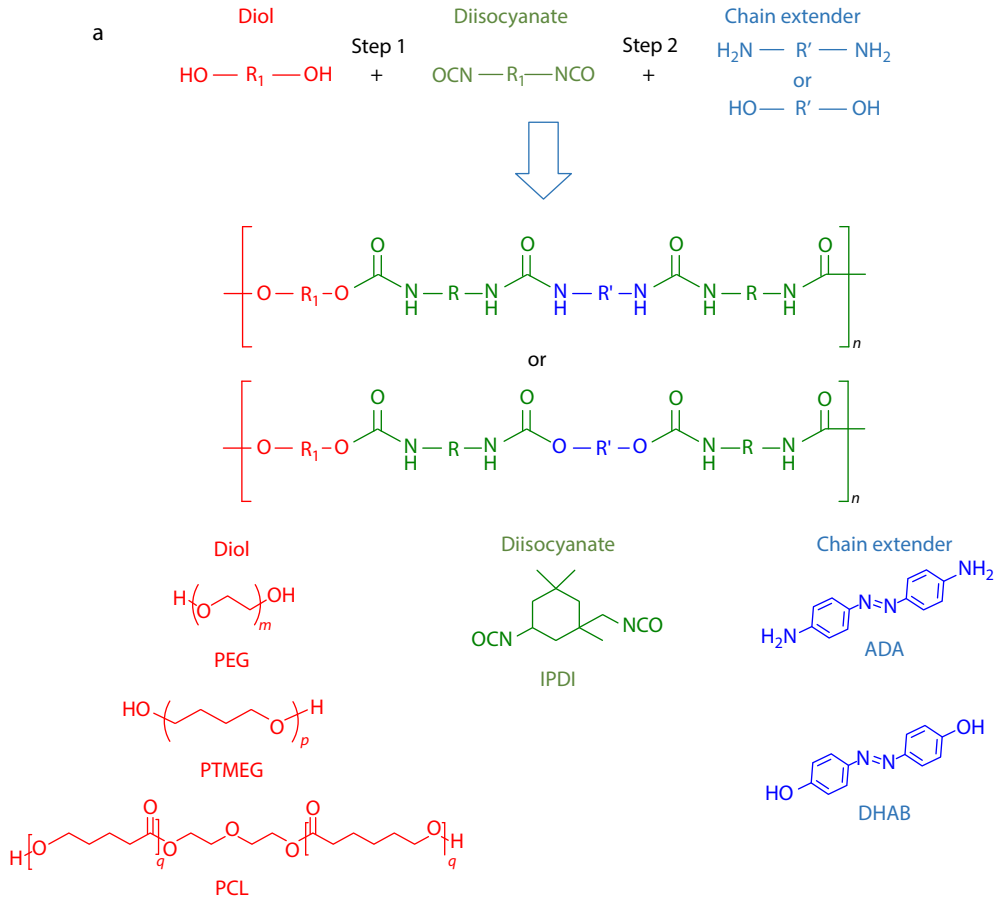

b

Sample	Composition	M_n	M_w	PDI
CPA	PCL-4k, IPDI, ADA	119k	213k	1.8
EPA	PEO-4k, IPDI, ADA	232k	393k	1.7
TPA	PTMEG-4k, IPDI, ADA	90k	156k	1.7
CPH	PCL-4k, IPDI, DHAB	155k	289k	1.9
EPH	PEO-4k, IPDI, DHAB	229k	428k	1.9
TPH	PTMEG-4k, IPDI, DHAB	124k	229k	1.8

c

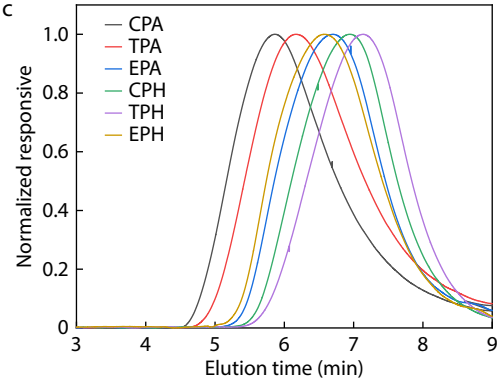

Scheme 1 (a) General synthesis and chemical structures, (b) detailed compositions, and (c) GPC traces of different polyurethanes.

with better microphase separation leading to slightly higher values. The same trend is well- documented for PTMEG systems. Hence, the pronounced crystallization differences between the "A" series and TPH/CPH series arise primarily from the chain extender chemistry that governs microphase separation and interphase hydrogen bonding, while the absolute crystallization temperature is set by the intrinsic structural regularity of the soft segment.

The mechanical behavior of polyurethane materials was investigated. Fig. 2 shows the stress-strain and load-unload curves of polyurethanes incorporating different soft segments and chain extenders. All the strips exhibited pronounced ductility, with TPH demonstrating the highest elongation at break and EPH having the lowest elongation. Notably, the tensile strengths of CPA and CPH, using polycaprolactone (PCL) as the soft segment, were significantly higher than those of their PEO-based and PTMEG-based counterparts. For example, the breaking stress of CPA approaches 27 MPa, whereas those of EPA and TPA approach about 18 and 13 MPa, respectively. Additionally, all polyurethane strips possess a relatively high initial modulus, followed by yielding, softening, and hardening, a phenomenon attributed to draw-induced molecular orientation and recrystallization. Upon unloading, partial elastic recovery was observed, although a significant plastic deformation persisted. 2D small-angle X-ray scattering (2D SAXS) patterns revealed that the microscopic

https://doi.org/10.1007/s10118-026-3757-8

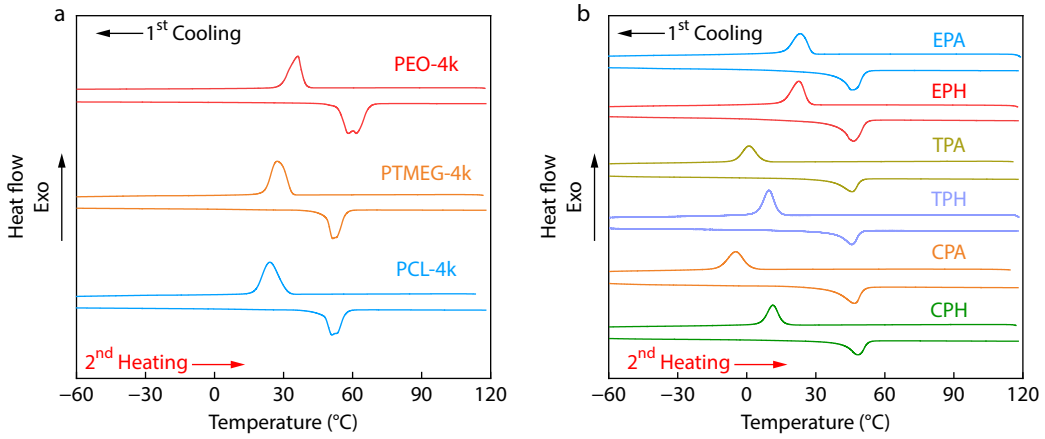

Fig. 1 DSC curves (first cooling and second heating) of (a) the diols PEO-4k, PTMEG-4k, PCL-4k and (b) the synthesized polyurethanes EPA, EPH, TPA, TPH, CPA and CPH.

Table 1 Melting peak temperature (T_m), crystallization peak temperature (T_c), and crystallinity (χ_c) of polyurethane samples and polyether/polyester diols.

Sample	Melting peak temperature (T_m, °C)	Crystallization peak temperature (T_c, °C)	Crystallinity (χ_c, %)
EPA	46	23	33.0
EPH	46	23	42.7
TPA	46	1.0	25.6
TPH	46	9.5	23.8
CPA	47	−5.0	31.9
CPH	48	11	28.4
PEO-4k	60	36	77.8
PTMEG-4k	50	27	39.5
PCL-4k	50	24	52.1

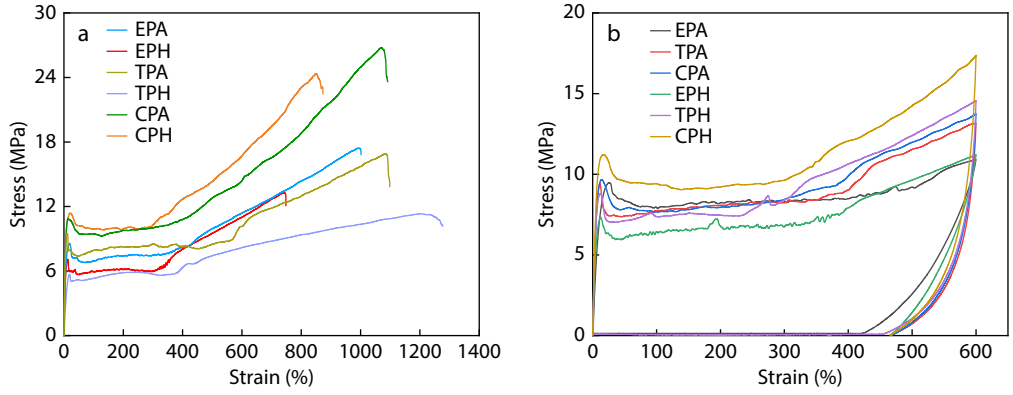

Fig. 2 (a) Stress-strain curves and (b) load-unload curves of EPA, EPH, TPA, TPH, CPA and CPH strips.

structures of all polyurethane strips were oriented after the cold-drawing process (Fig. S7 in ESI).

The distinct mechanical responses observed in the stress–strain curves originate from a combination of molecular and mesoscopic factors. At the molecular level, the intrinsic chemical structure of the soft segments dictates their intermolecular interactions. PEO, which contains only ether linkages, relies primarily on weak van der Waals forces, which facilitate segmental slippage under loading. PTMEG, with its longer tetramethylene sequence, exhibits reduced chain regularity and even weaker interchain cohesion, leading to the lowest mechanical strength among the three. In contrast, PCL soft segments possess highly polar ester groups that form strong dipole–dipole interactions, effectively restricting chain slippage and requiring greater energy for fracture. However, this molecular picture is insufficient to explain the pronounced performance gap between CPH and CPA, both of which incorporate the same PCL soft segment but differ in chain extender chemistry.

The SAXS analysis provides mesoscopic insights. The circular integration of the 2D scattering patterns reveals that CPH exhibits a notably stronger and sharper principal scattering peak in the low-q regime than CPA (Fig. S8c in ESI), suggesting a much higher degree of microphase separation between the soft and hard segments. This enhanced microphase segregation forces the PCL segments into "pure" soft domains with minimal hard segment dissolution. The purer PCL phase crystallized more readily and formed well-developed crys-

https://doi.org/10.1007/s10118-026-3757-8

talline lamellae. These crystallites act as both additional physical crosslinks and sacrificial energy-dissipating units, and their strain-induced reorganization and breakdown consume considerable energy during deformation. Moreover, the more ordered and segregated hard domains in the CPH undergo yielding and plastic deformation, which further contribute to energy dissipation. In CPA, inferior microphase separation leads to a phase-mixed soft phase with hindered PCL crystallization, depriving the material of these supplementary toughening mechanisms. Therefore, the superior mechanical performance of CPH arises synergistically from strong soft-segment intermolecular interactions and the reinforcing energy-dissipating morphology governed by the chain extender structure. In addition, we calculated the orientation indices for the stretched samples based on the relevant characterization data. The calculated results were 86.8% for TPH, 88.2% for CPH, 68.9% for TPA, and 65.7% for CPA. These data provide quantitative evidence for the structural evolution during the stretching process.

We then investigated the thermoresponsive behavior of the synthesized polyurethane materials. A 60 °C heat pipe was used as the heat source. All pristine polyurethane strips (denoted by '-p') exhibit no observable directional actuation behavior in 30 s towards the heat pipe (Fig. S9 in ESI). Upon stretching all six strips to a strain of 600%, all stretched strips (denoted by '-o') displayed distinct macroscopic actuation responses upon exposure to an external heat source, with all materials consistently bending towards the heat pipe (Figs. 3a–3f). Macroscopic deformation represents a one-time shape-recovery behavior because the elastic entropic energy stored during cold drawing was released during the first heat-induced actuation (Fig. S10 in ESI). Such different thermoresponsive behaviors can be explained by different microscopic structures. Pristine thin films prepared *via* solution casting exhibit isotropic aggregation states: the soft segments are randomly coiled, resulting in irregular chain alignment and non-oriented hard segments. Upon heating, thermal energy merely activates the random segmental motion of the soft

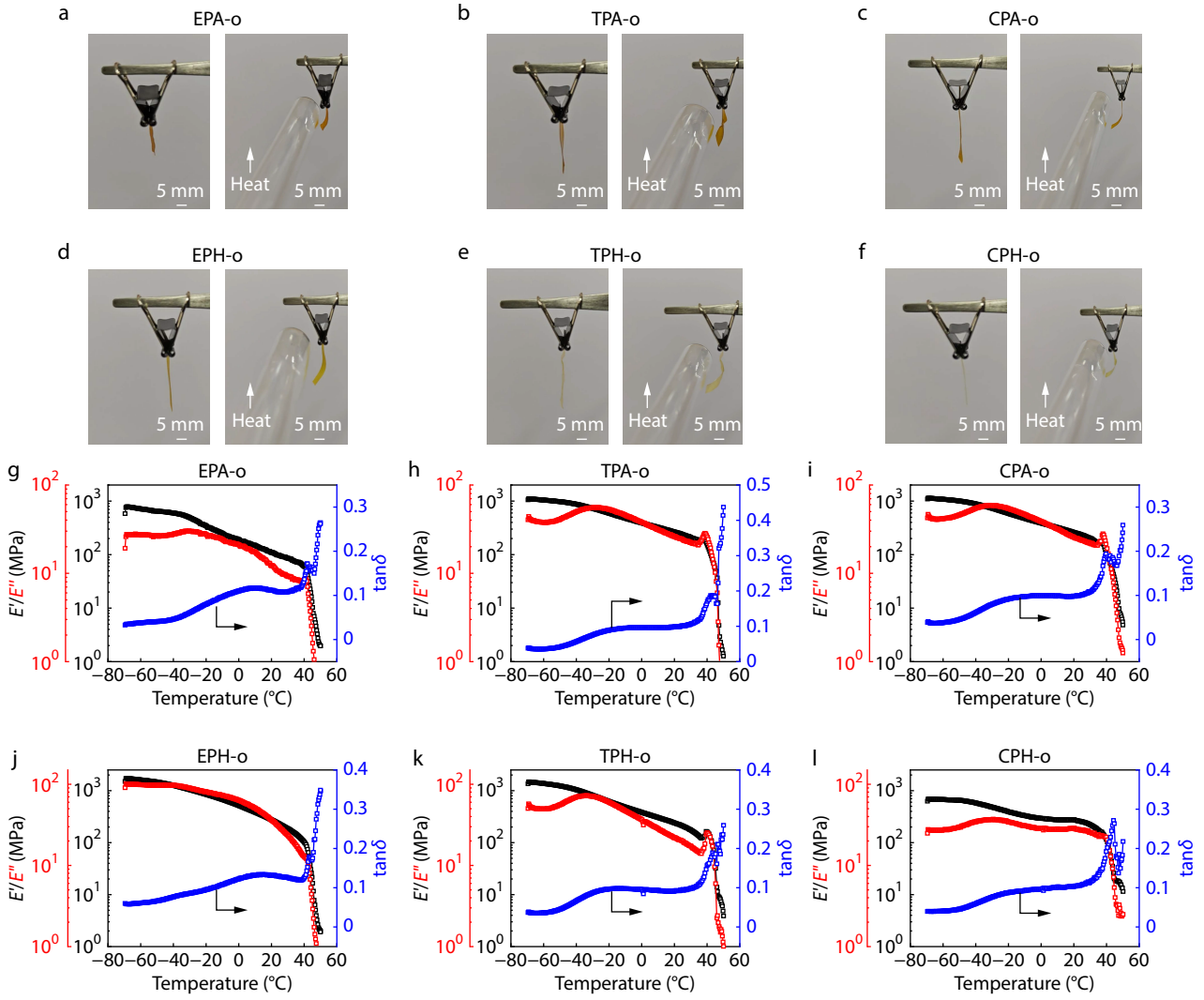

Fig. 3 Heat-responsive behaviors of the oriented (a) EPA, (b) TPA, (c) CPA strip, (d) EPH, (e) TPH and (f) CPH strips after exposing to heat source (a 60 °C heat pipe) for 30 s; DMA curves of (g) EPA, (j) EPH, (h) TPA, (k) TPH, (i) CPA and (l) CPH with temperature scan under dried air. (The online version is colorful.)

https://doi.org/10.1007/s10118-026-3757-8

segments, causing mutually cancelled extensions and contractions; hence, no directional actuation occurred. During stretching, molecular chains align along the stretch direction, with hard segments directionally aggregating and soft segments oriented, locking in an anisotropic structure because the melting temperatures are higher than room temperature. Upon heating, the soft segment chains revert to random coils, generating contraction along the orientation direction and releasing entropy elastic energy during stretching, resulting in observable bending deformation. Furthermore, the consistency of the bending direction (always towards the heat pipe) arises from a localized thermal gradient. As the heat pipe approaches the film, the surface facing the heat source rapidly absorbs thermal energy and first reaches the activation threshold for segmental mobility. Consequently, the highly oriented chains on this proximal surface initiate entropic contraction almost instantaneously, while the chains on the cooler and distal sides remain temporarily frozen in their extended state. This rapid asymmetric structural recovery creates a severe strain mismatch across the thickness of the film, generating a powerful localized bending moment that decisively curls the material towards the heat source.

The DMA temperature-sweep measurements of the stretched polyurethane films (Figs. 3g–3l) and pristine polyurethane films (Fig. S11 in ESI) further corroborated the significant impact of temperature on the stretched specimen. For all samples, the storage modulus (*E*′) remained high at low temperatures and then gradually decreased upon heating, indicating the progressive activation of segmental motion and weakening of the physically crosslinked network. Meanwhile, the loss modulus (*E*″) and tanδ increased with temperature and showed a pronounced increase in the vicinity of 40−50 °C, where *E*′ dropped sharply, suggesting a major relaxation process associated with the loss of stretch-induced orientation and the disruption of ordered microdomains. The results of the heat response first establish a fundamental prerequisite: none of the unstretched pristine specimens exhibited bending upon heating, whereas all oriented specimens (the -o series) underwent thermal bending in the same direction, but with distinctly different angles. This sharp contrast confirms that the molecular chain orientation along the stretching direction, accompanied by oriented crystallization, is a necessary condition for converting thermal energy into macroscopic directional actuation. Without such an oriented structure, the specimens can only undergo isotropic thermal expansion or softening, and are unable to generate a bending motion. The significant differences in the bending angles of the oriented specimens are primarily governed by the competition between the "driving force" arising from the oriented structure and the "stiffness resistance" of the material itself. The DMA curves show that EPA-o, TPA-o, and EPH-o not only possess a higher E' in the low-temperature region but also exhibit a more distinct modulus plateau, which reflects their higher degree of crystalline orientation and well-organized oriented lamellar structure. The enormous contractile driving force caused by the high degree of orientation significantly outweighs the accompanying increase in stiffness, thereby enabling the specimens to display larger bending angles. In contrast, CPH-o had the lowest initial *E*' and a much less pronounced modulus plateau, indicating a weaker degree of orientation and a looser structure. Consequently, the generated contractile driving force was insufficient, and its bending angle was the smallest.

Next, the photoresponsive behaviors of the polyurethane strips were investigated. It was found that after the cold-drawing treatment, the photoresponsive behaviors of the polyurethane strips changed significantly. The uniaxially oriented polyurethane strips exhibited pronounced bending upon UV irradiation for 30 s (Figs. 4a–4f), whereas the pristine strips did not (Fig. S12 in ESI). Both the polyurethanes bearing ADA and DHAB moieties exhibited similar photoresponsive behaviors. However, we found that the photoresponsive behaviors of ADA and DHAB in solution were significantly different, according to UV-Vis spectroscopy. The normal photoresponsive behavior of azobenzene-based materials is based on the *trans-cis* photoisomerization of azobenzene units upon UV irradiation.[56–59] Upon UV irradiation, the UV-Vis spectra of the DMF solutions of EPA, TPA, and CPA showed obvious changes in a few seconds (Figs. S11a–S11c in ESI), indicating the formation of a *cis*-isomer-rich state. However, the UV-Vis spectra of the DMF solutions of EPH, TPH, and CPH did not change after 60 min (Figs. S11d–S11f in ESI). The completely different photoresponsive behaviors of azobenzene-containing polyurethanes in the solution state and in the bulk state indicates that the photoresponsive mechanism of uniaxially oriented polyurethane strips is not simply based on normal *trans-cis* photoisomerization of azobenzene units upon UV irradiation.

To elucidate the photoresponsive mechanism of the oriented polyurethane strips, infrared thermal imaging was performed. Infrared thermal imaging results confirmed a significant increase in the surface temperature of the stretched strips upon UV irradiation. The initial state of the strips was shown in Figs. 4(g) and 4(j). After UV irradiation for 10 s, the surface temperatures of the samples increased significantly, with the maximum temperature of the EPA sample reaching 63.2 °C and that of the EPH sample reaching 79 °C (Figs. 4h and 4k), indicating a substantial photothermal effect. When the irradiation time increased to 30 s, the temperature of the EPH sample approached 160 °C, whereas the temperature of the EPA sample was 134.5 °C (Figs. 4i and 4l), exhibiting a larger temperature increase compared to that at 10 s of irradiation. Based on the infrared thermal imaging results and the consistent responsive behaviors of polyurethane strips towards light and heat stimuli, we propose that the photo-induced actuation of stretched polyurethane strips is dominated by the photothermal effect of azobenzene moieties and thermally induced actuation.[60–62] Macroscopic light-driven deformation is governed by an entropy-driven photothermal shape-memory effect, where temperature variations stem from a competitive allocation between photochemical and photothermal energy conversion pathways. In the 'H-series' materials (*e.g.*, EPH), the electron-donating effect of the oxygen atom drastically lowers the *cis-trans* thermal relaxation energy barrier. Upon the absorption of UV light by azobenzene chromophores, the absorbed photon energy is predominantly converted into thermal energy, leading to a rapid localized temperature rise. This sharp temperature increase in-

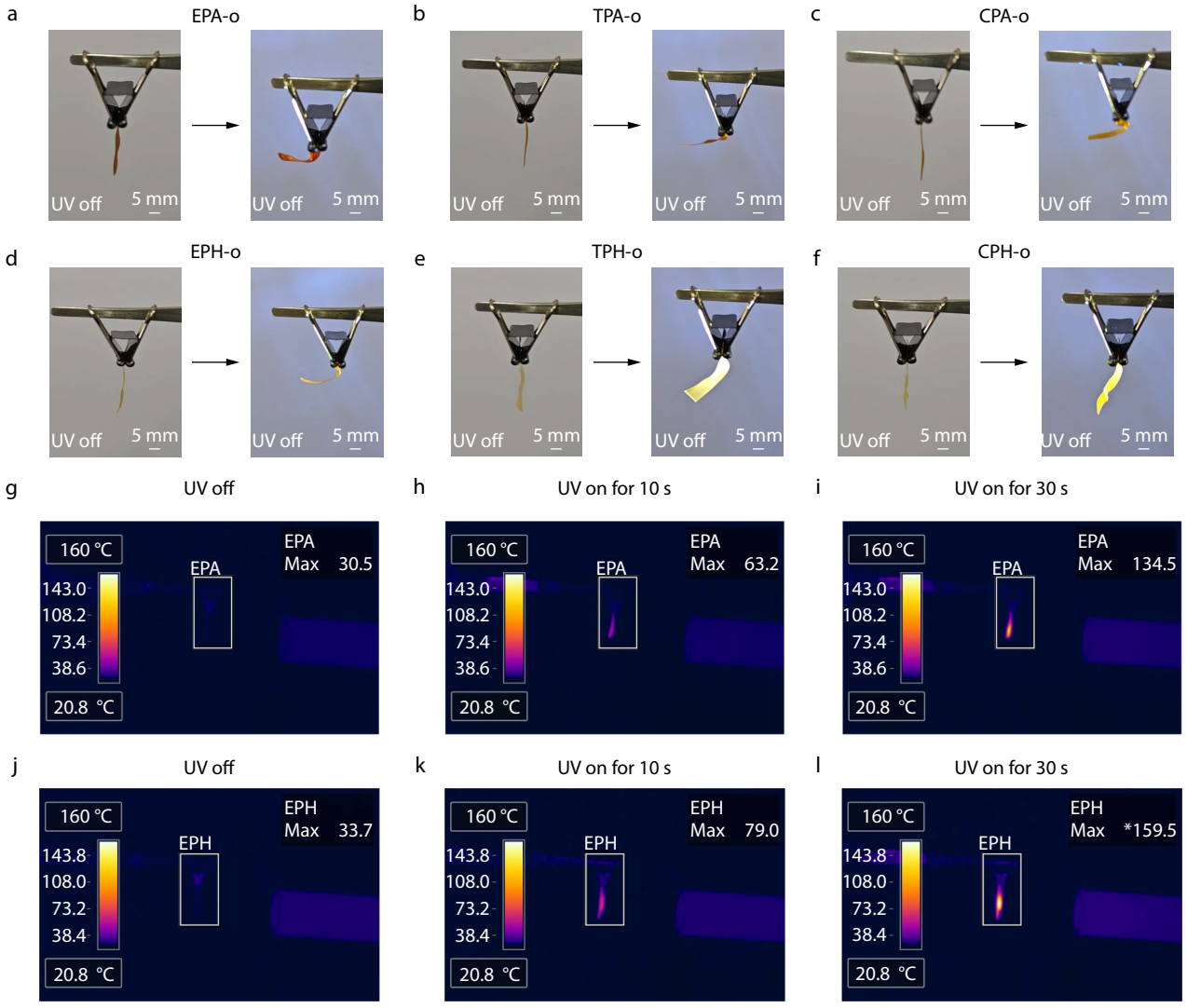

Fig. 4 Light-responsive behaviors of the oriented (a) EPA, (b) TPA, (c) CPA strip, (d) EPH, (e) TPH and (f) CPH strips by UV (λ = 365 nm) irradiation for 30 s; Infrared thermal imaging of the EPA strip: (g) UV off; (h) UV on for 10 s; (i) UV on for 30 s and EPH strip: (j) UV off; (k) UV on for 10 s; (l) UV on for 30 s.

duced by the photothermal effect enhances the mobility of the highly oriented soft segment chains, forcing the polymer chains to spontaneously retract towards a higher-entropy random coil state, thereby resulting in consistent macroscopic light-driven deformation. In contrast, the ADA-based series (*e.g.*, EPA) yields relatively stable *cis*-isomers; thus, a portion of the absorbed photon energy is successfully trapped as photochemical potential energy, leaving less energy to be dissipated as heat. Ultimately, in both systems, this rapid photothermal heating surpasses the thermal transition threshold, unlocking the mobility of the highly oriented soft segment chains and forcing them to spontaneously retract towards a higher-entropy random-coil state. This energy-partitioning mechanism elegantly reconciles why the 'H-series' materials exhibit superior photothermal heating and robust macroscopic actuation despite the absence of observable steady-state photoisomerization.

In Fig. 4, the fact that EPH reaches approximately 160 °C after 30 s of UV irradiation inevitably raises concerns the thermal aging of the material. Our results indicate that a short 30-second high-temperature exposure does not lead to thermal aging or mechanical deterioration. Instead, it acts as an "ultrafast photothermal annealing" process that enhances the mechanical properties of EPH films. To further verify this, we carried out additional tensile tests, DSC and Fourier transform infrared spectrometer (FTIR) measurements on the EPH strips after UV irradiation. Tensile stress-strain curves show that after 30 s of UV irradiation and cooling, the EPH film undergoes no mechanical deterioration; instead, tensile strength rises from *ca.* 13.5 MPa to *ca.* 17.5 MPa and elongation at break from *ca.* 750% to *ca.* 900% (Fig. S14 in ESI). This macroscopic "double enhancement" directly demonstrates that no thermal degradation occurred. FTIR confirmed that hard segments reassembled into a dense H-bonded network (Fig. S15 in ESI), while DSC revealed that PEO soft segments recrystallized into smaller, more uniform crystallites (Fig. S16 in ESI), together explaining the simultaneous enhancement in strength and elongation.

https://doi.org/10.1007/s10118-026-3757-8

Humidity is a key environmental parameter that significantly affects material properties.[52,63–67] Humidification was applied to the EPA, EPH, TPA, TPH, CPA, and CPH strips (Fig. 5, Fig. S17 in ESI). The EPA-p and EPH-p strips bent away from the moisture direction, while the TPA-p, TPH-p, CPA-p, and CPH-p strips showed no response to the humidity (Figs. S14a–S14f in ESI). The EPA-o and EPH-o strips bent towards the moisture flow, while the TPA-o, TPH-o, CPA-o, and CPH-o strips still showed no response to the humidity (Figs. 5a–5f). In general, the stretched PEO-based strips exhibited excellent initial humidity sensitivity, achieved deformation quickly, and reached their actuation limit in a short time (Fig. S18a in ESI). The contrasting humidity responses observed between the PEO-based (EPA/EPH) and PTMEG- and PCL-based systems can be rationalized through a combination of thermodynamic and structural factors. In EPA/EPH systems, the PEO backbone is densely populated with polar ether oxygen atoms, which readily form strong hydrogen bonds with water molecules. This thermodynamically favorable interaction overcomes the cohesive energy that holds the polymer chains together, leading to the spontaneous and substantial permeation of water into the network. The absorbed water acts as an efficient plasticizer and induces a "water-induced melting" of the PEO microcrystalline domains. The resulting complete disintegration of the crystalline crosslinked network eliminates the structural reinforcement that governs the stiffness of the material, thus serving as the microscopic origin of the drastic drop in the storage modulus (E') recorded under high-humidity conditions. In stark contrast, PTMEG- and PCL-based materials are constructed from long alkyl chains (PTMEG) or ester groups separated by extended alkyl segments (PCL), which render the chains strongly hydrophobic. The molecular cohesive energy within these systems was sufficiently high to resist the ingress of external water molecules. Consequently, the crystalline regions in these hydrophobic systems remain isolated from moisture, preserving their structural integrity. Without significant water uptake, neither plasticization nor crystalline disintegration occurs.

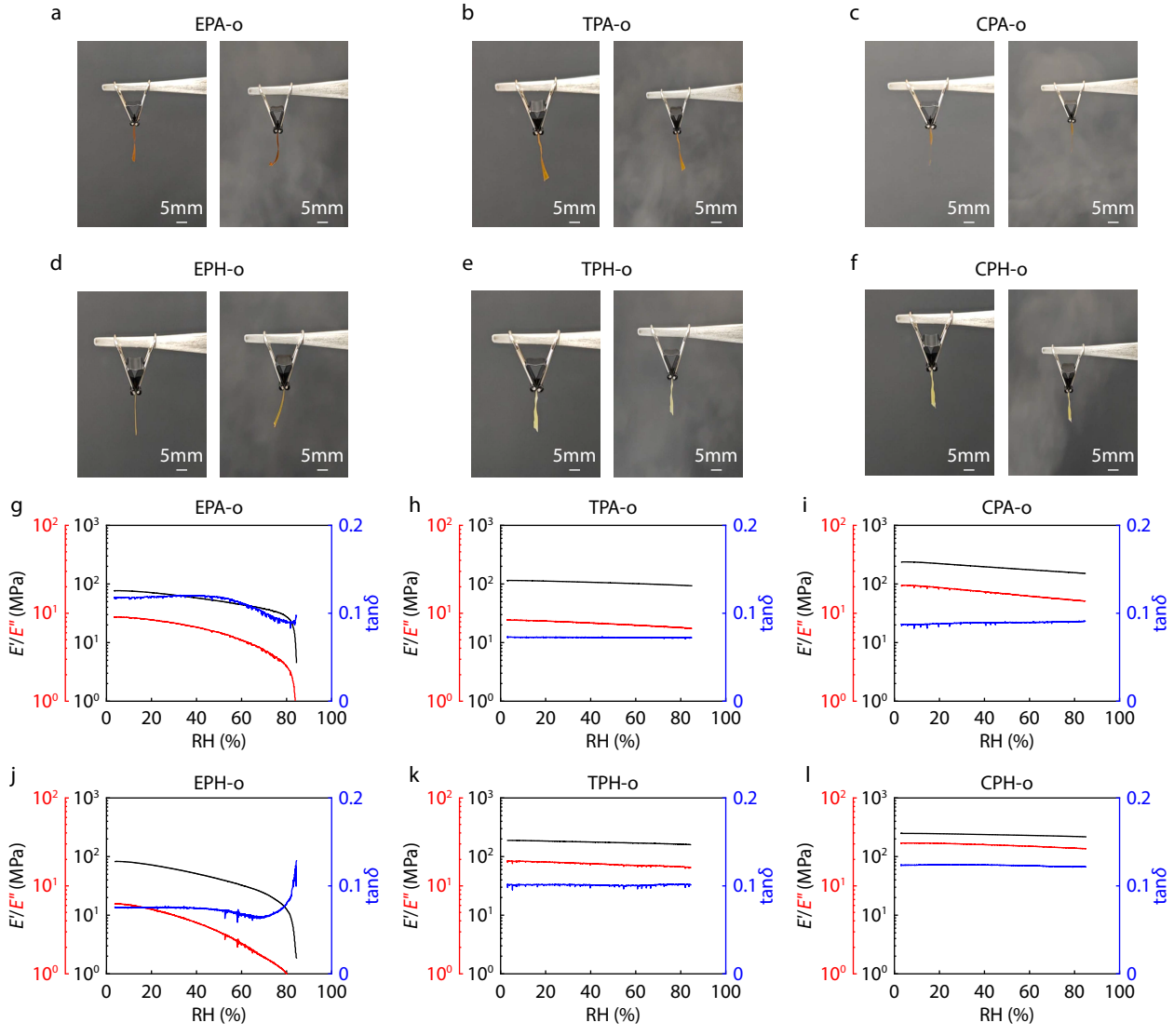

Fig. 5 Humidity-responsive behaviors of the oriented (a) EPA, (b) TPA, (c) CPA strips, (d) EPH, (e) TPH and (f) CPH strips. DMA curves of (g) EPA, (h) EPH, (i) TPA, (j) TPH, (k) CPA and (l) CPH with humidity scan at 25 °C. (The online version is colorful.)

https://doi.org/10.1007/s10118-026-3757-8

Table 2 Summary of multi-stimuli responsive behaviors of pristine and oriented polyurethane strips.

Sample	Light-response		Heat-response		Humidity-response	
	Direction	Bending angle	Direction	Bending angle	Direction	Bending angle
EPA-p	×	No	×	No	√→	34°
EPA-o	√←	84°	√←	20°	√←	17°
TPA-p	×	No	×	No	×	No
TPA-o	√←	75°	√←	15°	×	No
CPA-p	×	No	×	No	×	No
CPA-o	√←	66°	√←	23°	×	No
EPH-p	×	No	×	No	√→	37°
EPH-o	√←	76°	√←	15°	√←	17°
TPH-p	×	No	×	No	×	No
TPH-o	√←	50°	√←	28°	×	No
CPH-p	×	No	×	No	×	No
CPH-o	√←	27°	√←	22°	×	No

√ : Bending; × : No Bending; ← / → : Bending towards / away stimulus direction.

The crystalline network continues to provide stable mechanical reinforcement, yielding a storage modulus that is nearly insensitive to changes in ambient humidity. This order of hydrophilicity was further confirmed by the dynamic vapor sorption (DVS) of different polyurethanes (Fig. S18b in ESI). The DVS curve of EPA revealed a stepwise mass increase from the initial weight over time, achieving a remarkable weight gain of about 16.5%. Conversely, TPA and CPA exhibited a negligible weight gains of only about 0.54% and 0.14%. These findings further confirmed that the moisture sorption capacity of polyurethanes is dictated by the chemical structure and polarity of their soft segments.

The different bending directions of the pristine and oriented strips can be explained by their distinct humidity response mechanisms. For pristine strips EPA-p and EPH-p, the humidity response follows an 'adsorption-swelling' mechanism: the surface exposed to moisture rapidly adsorbs water and swells, creating a strain mismatch that drives bending away from moisture. The PEO soft segments were highly stretched for EPA-o and EPH-o. When approaching moisture, the highly stretched PEO chains on the moisture-facing surface tend to revert to random coils, thereby releasing the entropic elastic energy stored during cold drawing. This relaxation leads to size contraction of the moisture-facing surface, producing a strain mismatch that drives bending towards moisture. Fig. S18 (in ESI) a shows the bending angle-time curve of EPA-o. When a humidity stimulus is applied to the material surface, water molecules are first rapidly adsorbed onto the surface layer and induce the segmental motion of PEO, resulting in volume shrinkage of the surface layer and release of the elastic entropic energy. At this stage, the bending angle increased rapidly. Subsequently, water molecules diffused into the bulk of the strip, inducing further actuation accompanied by a slower increase in the bending angle. After 20 s of moisture exposure, the bending angle of EPA-o plateaued at approximately 34°.

The different humidity sensitivities of the polyurethane materials were also revealed by DMA with a humidity scan (Figs. 5g–5l, Fig. S14 in ESI). The PEO-based polyurethanes showed the strongest humidity sensitivity, with the storage modulus progressively decreasing with increasing RH and a pronounced reduction in loss modulus (Figs. 5g and 5j), indicating substantial water-induced plasticization of the polymer network. In particular, EPH-o displayed a sharp increase in tanδ at high RH, suggesting that moisture uptake activated significant segmental relaxation and drove the material towards a highly dissipative viscoelastic state. In contrast, the PTMEG-based and PCL-based polyurethanes exhibited nearly invariant storage modulus, loss modulus, and tanδ over the full humidity range (Figs. 5h–5i and 5k–5l), demonstrating excellent resistance to moisture-induced softening, indicating that the phase-separated structure remained largely unaffected by water. Overall, these results further demonstrate that the humidity responsiveness is governed primarily by the hydrophilicity of the soft segments.

The actuation behaviors of EPA, EPH, TPA, TPH, CPA, and CPH in response to light, heat, and humidity are summarized in Table 2. Only the EPA-o and EPH-o strips simultaneously exhibited light, heat, and humidity responses. The EPA-p and EPH-p strips responded to humidity, whereas the TPA-p, TPH-p, CPA-p, and CPH-p strips showed no response to the three stimuli. It is noteworthy that regardless of whether the EPA and EPH strips are stretched, they all show a response to humidity, although in opposite bending directions. To summarize, the multi-stimuli responsiveness of polyurethane strips is governed by molecular architecture and morphology: azobenzene moieties and chain orientation together enable light and heat responses, and hydrophilic soft segments govern humidity sensitivity.

CONCLUSIONS

In summary, through rational molecular design, we synthesized a series of responsive polyurethanes by integrating polyether/polyester soft segments with azobenzene-based chain extenders. Although these soft segments exhibit reduced crystallinity compared with neat diols, their retained crystallinity is sufficiently high to display ambient ductility, which enables cold drawing to induce the orientation of their microscopic structures. After the polyurethane materials were fabricated into test strips and stretched, all strips exhibited a directional actuation response towards external heat and UV light sources. A photoresponsive actuation mechanism dominated by the photothermal effect of azobenzene moieties and thermally induced actuation was revealed. Additionally, only the polyurethane strips with PEO soft segments showed actuation response to humidity, which is attributed to the inherent excellent hy-

drophilicity of PEO. Accordingly, polyurethanes incorporating PEO segments, azobenzene groups, and oriented structures show light, heat, and humidity triple-stimuli-responsive bending deformations and are endowed with the potential for designing programmable multi-mode sensing and actuation.

Conflict of Interests

The authors declare no interest conflict.

Electronic Supplementary Information

Electronic supplementary information (ESI) is available free of charge in the online version of this article at http://doi.org/10.1007/s10118-026-3757-8.

Data Availability Statement

The data supporting the findings of this study are available from the corresponding author upon reasonable request. Author's contact information: guoqy@dhu.edu.cn; shgyang@dhu.edu.cn.

ACKNOWLEDGMENTS

This work was financially supported by the National Natural Science Foundation of China (No. 52273020) and Shanghai Leading Talent Program of the Eastern Talent Plan.

REFERENCES

1 Zhang, K. Y.; Liu, S.; Zhao, Q.; Huang, W. Stimuli–responsive metallopolymers. *Coord. Chem. Rev.* **2016**, *319*, 180–195.
2 Santos, A.; Balderrama, V. S.; Alba, M.; Formentín, P.; Ferré-Borrull, J.; Pallarès, J.; Marsal, L. F. Nanoporous Anodic alumina barcodes: towards smart optical biosensors. *Adv. Mater.* **2012**, *24*, 1050–1054.
3 Rogóż, M.; Zeng, H.; Xuan, C.; Wiersma, D. S.; Wasylczyk, P. Light-Driven soft robot mimics caterpillar locomotion in natural scale. *Adv. Opt. Mater.* **2016**, *4*, 1689–1694.
4 Sagara, Y.; Yamane, S.; Mitani, M.; Weder, C.; Kato, T. Mechanoresponsive luminescent molecular assemblies: an emerging class of materials. *Adv. Mater.* **2016**, *28*, 1073–1095.
5 Mackanic, D. G.; Kao, M.; Bao, Z. Enabling deformable and stretchable batteries. *Adv. Energy Mater.* **2020**, *10*, 2001424.
6 Roach, D. J.; Yuan, C.; Kuang, X.; Li, V. C. F.; Blake, P.; Romero, M. L.; Hammel, I.; Yu, K.; Qi, H. J. Long liquid crystal elastomer fibers with large reversible actuation strains for smart textiles and artificial muscles. *ACS Appl. Mater. Interfaces.* **2019**, *11*, 19514–19521.
7 Hu, J.; Meng, H.; Li, G.; Ibekwe, S. I. A review of stimuli-responsive polymers for smart textile applications. *Smart Mater. Struct.* **2012**, *21*, 053001.
8 Pilz da Cunha, M.; Ambergen, S.; Debije, M. G.; Homburg, E. F. G. A.; den Toonder, J. M. J.; Schenning, A. P. H. J. A soft transporter robot fueled by light. *Adv. Sci.* **2020**, *7*, 1902842.
9 Lugger, S. J. D.; Houben, S. J. A.; Foelen, Y.; Debije, M. G.; Schenning, A. P. H. J.; Mulder, D. J. Hydrogen-bonded supramolecular liquid crystal polymers: smart materials with stimuli-responsive, self-healing, and recyclable properties. *Chem. Rev.* **2022**, *122*, 4946–4975.
10 Ma, Y.; She, P.; Zhang, K. Y.; Yang, H.; Qin, Y.; Xu, Z.; Liu, S.; Zhao, Q.; Huang, W. Dynamic metal-ligand coordination for multicolour and water-jet rewritable paper. *Nat. Commun.* **2018**, *9*, 3.
11 She, P.; Qin, Y.; Wang, X.; Zhang, Q. Recent progress in external-stimulus-responsive 2D covalent organic frameworks. *Adv. Mater.* **2022**, *34*, 2101175.
12 Wang, J.; Zhao, Q.; Wang, Y.; Zeng, Q.; Wu, T.; Du, X. Self-unfolding flexible microelectrode arrays based on shape memory polymers. *Adv. Mater. Technol.* **2019**, *4*, 1900566.
13 Huang, Y.; Ning, L.; Zhang, X.; Zhou, Q.; Gong, Q.; Zhang, Q. Stimuli-fluorochromic smart organic materials. *Chem. Soc. Rev.* **2024**, *53*, 1090–1166.

Graphical Abstract

Multi-stimuli Responsive Polyurethane-based Materials: Structure-Property Correlations

Yi-Sheng Huang, Han-Xin Jian, Hao Huang, Qing-Yun Guo, and Shu-Guang Yang

Donghua University

Heat-, light-, and humidity-responsive polyurethanes were developed by incorporating azobenzene into crystallizable soft segments. Cold-drawing stores entropic elastic energy, which is released upon heating, UV irradiation (*via* the photothermal effect), or moisture, driving distinct bending behaviors. This molecular design and post-processing synergy enabled the development of advanced multi-stimuli-responsive actuators.

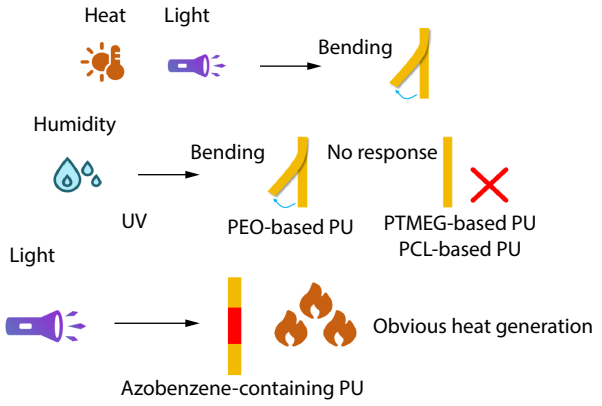

Chinese J. Polym. Sci., 2026 *https://doi.org/10.1007/s10118-026-3757-8*

14 Yang, P.; Zhu, F.; Zhang, Z.; Cheng, Y.; Wang, Z.; Li, Y. Stimuli-responsive polydopamine-based smart materials. *Chem. Soc. Rev.* **2021**, *50*, 8319–8343.
15 Xiao, Y. Y.; Jiang, Z. C.; Tong, X.; Zhao, Y. Biomimetic locomotion of electrically powered "Janus" soft robots using a liquid crystal polymer. *Adv. Mater.* **2019**, *31*, 1903452.
16 Yang, Q.; Peng, C.; Ren, J.; Zhao, W.; Zheng, W.; Zhang, C.; Hu, Y.; Zhang, X. A near-infrared photoactuator based on shape memory semicrystalline polymers towards light-fueled crane, grasper, and walker. *Adv. Opt. Mater.* **2019**, *7*, 1900784.
17 Huang, T.; Su, Z.; Hou, K.; Zeng, J.; Zhou, H.; Zhang, L.; Nunes, S. P. Advanced stimuli-responsive membranes for smart separation. *Chem. Soc. Rev.* **2023**, *52*, 4173–4207.
18 Zhuang, J.; Gordon, M. R.; Ventura, J.; Li, L.; Thayumanavan, S. Multi-stimuli responsive macromolecules and their assemblies. *Chem. Soc. Rev.* **2013**, *42*, 7421–7435.
19 Jochum, F. D.; Theato, P. Temperature- and light-responsive smart polymer materials. *Chem. Soc. Rev.* **2013**, *42*, 7468–7483.
20 Li, X.; Cai, X.; Gao, Y.; Serpe, M. J. Reversible bidirectional bending of hydrogel-based bilayer actuators. *J. Mater. Chem. B.* **2017**, *5*, 2804–2812.
21 Yamada, M.; Kondo, M.; Mamiya, J.-i.; Yu, Y.; Kinoshita, M.; Barrett, C. J.; Ikeda, T. Photomobile polymer materials: towardss light-driven plastic motors. *Angew. Chem. Int. Ed.* **2008**, *47*, 4986–4988.
22 Zhang, C.; Zhang, Z.; Liu, X. Closed-loop recyclable and totally renewable liquid crystal networks with room-temperature programmability and reconfigurable functionalities. *Angew. Chem. Int. Ed.* **2024**, *63*, e202411280.
23 Lang, C.; Lloyd, E. C.; Matuszewski, K. E.; Xu, Y.; Ganesan, V.; Huang, R.; Kumar, M.; Hickey, R. J. Nanostructured block copolymer muscles. *Nat. Nanotechnol.* **2022**, *17*, 752–758.
24 Yao, X.; Chen, H.; Qin, H.; Wu, Q. H.; Cong, H.-P.; Yu, S.-H. Solvent-adaptive hydrogels with lamellar confinement cellular structure for programmable multimodal locomotion. *Nat. Commun.* **2024**, *15*, 9254.
25 Guan, G.; Wu, M.; Han, M. Y. Stimuli-responsive hybridized nanostructures. *Adv. Funct. Mater.* **2020**, *30*, 1903439.
26 Wei, M.; Gao, Y.; Li, X.; Serpe, M. J. Stimuli-responsive polymers and their applications. *Polym. Chem.* **2017**, *8*, 127–143.
27 Hu, L.; Wan, Y.; Zhang, Q.; Serpe, M. J. Harnessing the power of stimuli-responsive polymers for actuation. *Adv. Funct. Mater.* **2020**, *30*, 1903471.
28 Hu, L.; Zhang, Q.; Li, X.; Serpe, M. J. Stimuli-responsive polymers for sensing and actuation. *Mater. Horiz.* **2019**, *6*, 1774–1793.
29 Yan, H.; Jiang, Q.; Wang, J.; Cao, S.; Qiu, Y.; Wang, H.; Liao, Y.; Xie, X. A triple-stimuli responsive supramolecular hydrogel based on methoxy-azobenzene-grafted poly(acrylic acid) and β-cyclodextrin dimer. *Polymer* **2021**, *221*, 123617.
30 Chikh Alard, I.; Soubhye, J.; Berger, G.; Gelbcke, M.; Spassov, S.; Amighi, K.; Goole, J.; Meyer, F. Triple-stimuli responsive polymers with fine tuneable magnetic responses. *Polym. Chem.* **2017**, *8*, 2450–2456.
31 Li, X.; Han, J.; Wang, X.; Zhang, Y.; Jia, C.; Qin, J.; Wang, C.; Wu, J.-R.; Fang, W.; Yang, Y. W. A triple-stimuli responsive hormone delivery system equipped with pillararene magnetic nanovalves. *Mater. Chem. Front.* **2019**, *3*, 103–110.
32 Yan, H.; Wang, J.; He, X.; Yu, D.; Qiu, Y.; Liao, Y.; Xie, X. A quadruple-stimuli responsive supramolecular hydrogel constructed from a poly(acrylic acid) derivative and β-cyclodextrin dimer. *Soft Matter* **2024**, *20*, 5343–5350.
33 Chen, Y.; Li, H.; Zhang, Y.; Li, Z.; Yang, D. Eu^{3+}-directed supramolecular metallogels with reversible quadruple-stimuli response behaviors. *Small* **2024**, *20*, 2309542.
34 Yang, J.; Dai, D.; Lou, X.; Ma, L.; Wang, B.; Yang, Y.-W. Supramolecular nanomaterials based on hollow mesoporous drug carriers and macrocycle-capped CuS nanogates for synergistic chemo-photothermal therapy. *Theranostics* **2020**, *10*, 615–629.
35 Shang, J.; Theato, P. Smart composite hydrogel with pH-, ionic strength- and temperature-induced actuation. *Soft Matter* **2018**, *14*, 8401–8407.
36 Huang, X.; Jiang, X.; Yang, Q.; Chu, Y.; Zhang, G.; Yang, B.; Zhuo, R. Triple-stimuli (pH/thermo/reduction) sensitive copolymers for intracellular drug delivery. *J. Mater. Chem. B* **2013**, *1*, 1860–1868.
37 Xu, W.; Qian, J.; Hou, G.; Wang, Y.; Wang, J.; Sun, T.; Ji, L.; Suo, A.; Yao, Y. A dual-targeted hyaluronic acid-gold nanorod platform with triple-stimuli responsiveness for photodynamic/photothermal therapy of breast cancer. *Acta Bio.* **2019**, *83*, 400–413.
38 Zhang, X.; Gao, J.; Zhao, X.; Liu, Z.; Liu, Z.; Wang, K.; Li, G.; Jiang, J. Hyperbranched polymer micelles with triple-stimuli backbone-breakable iminoboronate ester linkages. *Chinese Chem. Lett.* **2020**, *31*, 1822–1826.
39 Gao, W.; Bigham, A.; Ghomi, M.; Zarrabi, A.; Rabiee, N.; Saeb, M. R.; Nuri Ertas, Y.; Goel, A.; Sharifi, E.; Ashrafizadeh, M.; Sethi, G.; Tambuwala, M. M.; Wang, Y.; Ghaffarlou, M.; Jiao, T. Micelle-engineered nanoplatforms for precision oncology. *Chem. Eng. J.* **2024**, *495*, 153438.
40 Mei, G.; Su, Z.; Liu, N.; Qu, J.; Liu, X.; Qian, D.; Zhou, X.; Liu, Z. Robust artificial spider silk *via* synergistic cross-linking of slide-ring and covalent bonds. *Macromolecules* **2025**, *58*, 10738–10751.
41 Li, J.; Mei, G.; Fang, S.; Liu, X.; Liu, S.; Liu, Y.; Yang, Z.; Han, X.; Wang, M.; Xiao, Y.; Chang, W.; Guo, W.; Zhao, W.; Zhang, G.; Zhang, Z.; Li, C.; Zhang, M.; Bai, J.; Zhou, X.; Baughman, R. H.; Liu, Z. Creating nanoknot-like domains for robust artificial spider silk towards high twistocaloric performance. *Adv. Mater.* **2026**, *38*, e16934.
42 Li, Z.; Zhu, Y.-L.; Niu, W.; Yang, X.; Jiang, Z.; Lu, Z.-Y.; Liu, X.; Sun, J. Healable and recyclable elastomers with record-high mechanical robustness, unprecedented crack tolerance, and superhigh elastic restorability. *Adv. Mater.* **2021**, *33*, 2101498.
43 McCune, J. A.; Mommer, S.; Parkins, C. C.; Scherman, O. A. Design principles for aqueous interactive materials: lessons from small molecules and stimuli-responsive systems. *Adv. Mater.* **2020**, *32*, 1906890.
44 He, W.; Wang, M.; Mei, G.; Liu, S.; Khan, A. Q.; Li, C.; Feng, D.; Su, Z.; Bao, L.; Wang, G.; Liu, E.; Zhu, Y.; Bai, J.; Zhu, M.; Zhou, X.; Liu, Z. Establishing superfine nanofibrils for robust polyelectrolyte artificial spider silk and powerful artificial muscles. *Nat. Commun.* **2024**, *15*, 3485.
45 Li, Y.; Schreiber, S.; Yang, H.; Liu, M.; Little, J. M.; Cao, W.; Luo, Y.; Bao, Y.; Shih, C. J.; Bai, H.; Chen, P. Y. From molecules to machines: a multiscale roadmap to intelligent, multifunctional soft robotics. *Chem. Rev.* **2025**, *125*, 8123–8245.
46 Kumar, N.; Singh, S.; Sharma, P.; Kumar, B.; Kumar, A. Single-, dual-, and multi-stimuli-responsive nanogels for biomedical applications. *Gels* **2024**, *10*, 61.
47 Wojtecki, R. J.; Meador, M. A.; Rowan, S. J. Using the dynamic bond to access macroscopically responsive structurally dynamic polymers. *Nat. Mater.* **2011**, *10*, 14–27.
48 Rice, A. M.; Martin, C. R.; Galitskiy, V. A.; Berseneva, A. A.; Leith, G. A.; Shustova, N. B. Photophysics modulation in photoswitchable metal-organic frameworks. *Chem. Rev.* **2020**, *120*, 8790–8813.
49 Zhu, S.; Wang, S.; Huang, Y.; Tang, Q.; Fu, T.; Su, R.; Fan, C.; Xia, S.; Lee, P. S.; Lin, Y. Bioinspired structural hydrogels with highly ordered hierarchical orientations by flow-induced alignment of nanofibrils. *Nat. Commun.* **2024**, *15*, 118.
50 Wang, L.; Li, Q. Photochromism into nanosystems: towardss lighting up the future nanoworld. *Chem. Soc. Rev.* **2018**, *47*,

1044–1097.
51 Nguyen, T. H. L.; Gigant, N.; Joseph, D. Advances in direct metal-catalyzed functionalization of azobenzenes. *ACS Catal.* **2018**, *8*, 1546–1579.
52 Jian, H.; Wang, W.; Yao, Y.; Yang, Y.; Huang, Y.; Huang, H.; Yang, S. Cold drawing of azobenzene incorporated poly(urethane urea)s for heat, humidity and light responsiveness. *Polymer* **2026**, *343*, 129449.
53 Tian, J.; Zhou, Z.; Miao, X.; Wang, S.; Ming, Y.; Nie, Y.; Ma, Y.; Li, Z. Supertough, resilient, and healable thermoplastic poly(urethane urea) elastomers by dense packing of hydrogen-bonding arrays. *Adv. Funct. Mater.* **2026**, *36*, e04882.
54 Wang, L.; Guo, L.; Zhang, K.; Xia, Y.; Hao, J.; Wang, X. Development of tough thermoplastic elastomers by leveraging rigid–flexible supramolecular segment interplays. *Angew. Chem. Int. Ed.* **2023**, *62*, e202301762.
55 Wang, X.; Xu, J.; Zhang, Y.; Wang, T.; Wang, Q.; Li, S.; Yang, Z.; Zhang, X. A stretchable, mechanically robust polymer exhibiting shape-memory-assisted self-healing and clustering-triggered emission. *Nat. Commun.* **2023**, *14*, 4712.
56 Bandara, H. M. D.; Burdette, S. C. Photoisomerization in different classes of azobenzene. *Chem. Soc. Rev.* **2012**, *41*, 1809–1825.
57 Gelebart, A. H.; Jan Mulder, D.; Varga, M.; Konya, A.; Vantomme, G.; Meijer, E. W.; Selinger, R. L. B.; Broer, D. J. Making waves in a photoactive polymer film. *Nature* **2017**, *546*, 632–636.
58 Hartley, G. S. The *cis*-form of azobenzene. *Nature* **1937**, *140*, 281–281.
59 Rau, H.; Lueddecke, E. On the rotation-inversion controversy on photoisomerization of azobenzenes. Experimental proof of inversion. *J. Am. Chem. Soc.* **1982**, *104*, 1616–1620.
60 Verpaalen, R. C. P.; Varghese, S.; Froyen, A.; Pilz da Cunha, M.; Pouderoijen, M. J.; Severn, J. R.; Bhatti, M. R.; Peijs, T.; Bastiaansen, C. W. M.; Debije, M. G.; Engels, T. A. P.; Schenning, A. P. H. J. Fast, light-responsive, metal-like polymer actuators generating high stresses at low strain. *Matter* **2020**, *2*, 1522–1534.
61 Bhatti, M. R. A.; Bilotti, E.; Zhang, H.; Bastiaansen, C. W. M.; Peijs, T. Photo-thermal actuation of ultra-drawn high-density polyethylene. *Polymer* **2020**, *207*, 122897.
62 Varghese, S.; Fredrich, S.; Vantomme, G.; Prabhu, S. R.; Teyssandier, J.; De Feyter, S.; Severn, J.; Bastiaansen, C. W. M.; Schenning, A. P. H. J. Epitaxial growth of light-responsive azobenzene molecular crystal actuators on oriented polyethylene films. *J. Mater. Chem. C.* **2020**, *8*, 694–699.
63 Liu, Z.; Huang, H.; Yin, P.; Zhang, C.; Yang, S. Dynamics of hydrogen-bonded polymer complexes of poly(ether oxide) and poly(acrylic acid): time-humidity-temperature equivalence. *Polymer* **2025**, *320*, 128080.
64 Huang, H.; Liu, Z.; Jian, H.; Yao, Y.; Tan, W.; Yang, S. Alginate/chitosan complex fibers reinforcement and their mechanical transition continuum with water uptake increasing. *Macromol. Rapid Commun.* **2025**, *46*, 2400735.
65 Wang, W.; Jian, H.; Huang, H.; Feng, F.; Meng, Q.; Li, Y.; Chen, G.; Yang, S. Structure, humidity adaptivity, and elasticity of hydrogen-bonded complexes formed by self-assembly of a triblock copolymer and a homopolymer. *Polym. Chem.* **2024**, *15*, 4710–4720.
66 Huang, H.; Liu, Z.; Jian, H.; Yao, Y.; Xue, B.; Yang, S. Humidity-adaptive behaviors of alginate/chitosan complex fiber. *ACS Appl. Polym. Mater.* **2024**, *6*, 4634–4641.
67 C. Zhang, W. Wang, H. Huang, Z. Liu, S. Yang. Effect of humidity on mechanical behavior of polymer hydrogen-bonding complex fibers. *Acta Polymerica Sinica* (in Chinese), **2023**, *54*, 1772–1783.

https://doi.org/10.1007/s10118-026-3757-8